Physics of the granite sphere fountain

Jacco H. Snoeijer and Ko van der Weele

Articles you may be interested in

Squeeze flow of a Carreau fluid during sphere impact
Phys. Fluids **24**, 073104 (2012); 10.1063/1.4736742

Rolling stones: The motion of a sphere down an inclined plane coated with a thin liquid film
Phys. Fluids **21**, 082103 (2009); 10.1063/1.3207884

Microrheology of model quasi-hard-sphere dispersions
J. Rheol. **48**, 117 (2004); 10.1122/1.1626678

Three-particle contribution to effective viscosity of hard-sphere suspensions
J. Chem. Phys. **119**, 606 (2003); 10.1063/1.1576378

Contribution to the Study of Viscous Friction and the Application to the Theory of Lubrication
J. Rheol. **3**, 391 (1932); 10.1122/1.2116504

Physics of the granite sphere fountain

Jacco H. Snoeijer
Physics of Fluids Group and J.M. Burgers Centre for Fluid Dynamics, University of Twente, P.O. Box 217, 7500 AE Enschede, The Netherlands

Ko van der Weele
Department of Mathematics, University of Patras, 26500 Patras, Greece

A striking example of levitation is encountered in the "kugel fountain" where a granite sphere, sometimes weighing over a ton, is kept aloft by a thin film of flowing water. In this paper, we explain the working principle behind this levitation. We show that the fountain can be viewed as a giant ball bearing and thus forms a prime example of lubrication theory. It is demonstrated how the viscosity and flow rate of the fluid determine (i) the remarkably small thickness of the film supporting the sphere and (ii) the surprisingly long time it takes for rotations to damp out. The theoretical results compare well with measurements on a fountain holding a granite sphere of one meter in diameter. We close by discussing several related cases of levitation by lubrication.
© 2014 American Association of Physics Teachers.
[http://dx.doi.org/10.1119/1.4886365]

I. INTRODUCTION

Granite sphere or "kugel" fountains (see Fig. 1) are a familiar sight in town squares and science museums, and smaller ones—often with a marble sphere—decorate many private homes and gardens. These fountains consist of a perfectly polished ball floating in a socket that fits precisely around it. The fluid that wells up around the rim of the socket is pumped into the fountain via a hole at the base. In spite of its considerable weight, the sphere is easily brought into a spinning motion, which is an attractive sight especially when the surface of the sphere is engraved with the Earth's map, a soccer ball, the night sky, or something of the kind. The fluid layer between the socket and sphere is very thin (thinner than a credit card[1]), which is important for any kugel on display in a public place, since it means there is no risk of children's fingers being caught under the spinning sphere.

Despite its popularity, the granite sphere fountain is poorly understood by most people. When we asked visitors of the House of Science in Patras, Greece, which physical mechanism they thought was responsible for the floating of the sphere in front of the main entrance (a granite ball with a diameter of 1 m), the most common answer was "Archimedes' law of buoyancy," as if the sphere were an iceberg or a ship. Perhaps the visitors who gave this answer were under the impression that the sphere was hollow. In reality, however, the sphere is solid and the buoyant force is by no means capable of keeping the sphere afloat, since granite has a density 2.75 times that of water.

The second most common answer was "the incompressibility of water." This is not too convincing either, because it fails to explain why the sphere does not squeeze the water out of the space between itself and the socket and simply sit on top of the inlet nozzle like a giant granite plug.

A third answer was "Pascal's principle," which states that a pressure applied to an enclosed incompressible fluid at rest is transmitted undiminished and isotropically to every part of the fluid, as well as to the walls of the container. This comes much closer to the truth, as we will see, even though the water in the fountain is neither fully enclosed (it is open at the rim of the socket) nor at rest.

A search on the internet did not yield much in the way of a conclusive answer. On the website of one of the leading manufacturers of these fountains, it is stated that "basic physical principles and very accurate working of the stone allow granite objects weighing tons to float on air or water,"[2] without giving any hint as to what these basic principles are. Another website, describing the Millennium Globe in Kenilworth, UK, says that "complex physics and precision engineering" are involved.[3] The description on wikipedia about the *kugel ball*, as the fountain is widely known (from the German "Kugel," meaning bullet or ball), states that the sphere is supported by a very thin film of water and "because the thin film of water lubricates it, the ball spins."[4] Finally, we came across several physics forums where students asked about the working of the kugel fountain without getting any answer that went much deeper than the above statements.

In our view, therefore, there is some reason for a paper that explains the physics of the granite sphere fountain. It turns out that the levitation hinges on the principle of lubrication. The key observation is that the pressure that builds up in the thin fluid layer, squeezed as it is between the kugel and the socket, supplies the force required to balance the

Fig. 1. One of the largest granite sphere fountains in the world, the Grand Kugel at the Science Museum of Virginia, in Richmond, VA. The sphere has a diameter of 2.65 m and a mass of about 27 tons.

colossal weight of the granite sphere. The pressure integrated over the submerged area gives an upward force that equals the weight of the sphere plus the force exerted by the atmospheric pressure on the equivalent area around the top. For the sake of clarity, we neglect buoyancy and also the minor contribution to the upward force from the shear stresses at the submerged surface of the kugel. Hence, if F_g is the weight of the sphere and F_{up} the resultant upward force due to the pressure inside the fluid layer minus the atmospheric counterforce, the balance gives

$$F_g = F_{up} = \iint_{\mathcal{A}_{sub}} [P(\theta) - P_{atm}] \cos \theta \, dA, \tag{1}$$

where $\mathcal{A}_{sub}$ denotes the submerged area of the sphere. The angle θ appearing in this relation runs from 0 at the center of the fountain's basin to θ_{max} at the rim. In the next sections, we will work out Eq. (1) in detail, but we can already make a back-of-the-envelope estimate right here.

For a granite sphere with a diameter of $1\,m$, the mass is $m = (4/3)\pi R^3 \rho_{gr} = 1440\,kg$ (with $R = 0.5\,m$ and $\rho_{gr} = 2750\,kg/m^3$), so its weight is $F_g = mg \approx 1.4 \times 10^4\,N$. Given that the submerged area of such a sphere will be approximately $\mathcal{A}_{sub} \approx 1.5\,m^2$, the average fluid overpressure (above atmospheric pressure) on this surface must be $1.4 \times 10^4\,N/1.5\,m^2 = 0.93 \times 10^4\,N/m^2 \approx 0.1\,atm$. Thus, with the pressure at the rim of the socket (where the water meets the surrounding air) being $1\,atm$, the pressure under the sphere must exceed this on average by $0.1\,atm$. Thus, a surprisingly low pressure is required to make the fountain work. The excess pressure above atmospheric pressure ($0.1\,atm$) is usually called *gauge pressure*, and the total pressure ($1.1\,atm$) is called *absolute pressure*. In the present work, we must take care to distinguish between these two quantities. The absolute pressure will be denoted by P, the gauge pressure by $P - P_{atm}$ [as in Eq. (1)].

The remainder of this paper is organized as follows. In Sec. II, we first turn our attention to the *cylindrical* version of the Kugel fountain and, performing the above calculation in more detail, we will see that it is in fact a beautiful exercise in lubrication theory. This calculation may well find its way into the classroom as part of an introductory course in fluid dynamics. In Sec. III, we analyze the *spherical* fountain, which is slightly more advanced both from a mathematical and a physical point of view. In Sec. IV, we address the spinning motion of the sphere and especially the rate with which the rotations damp out due to the viscosity in the fluid layer. Finally, in Sec. V, we discuss the analogies between the granite sphere fountain and other instances in which objects are levitated by a thin fluid layer, such as water drops floating on their own vapor layer above an overheated surface (the so-called Leidenfrost phenomenon) and also the air-borne variety of the kugel fountain.

II. CYLINDRICAL FOUNTAIN

We first consider a two-dimensional version of the fountain where the levitated object is a cylinder instead of a sphere. This is known as the "granite wheel," an example of which is shown in Fig. 2. The analysis for the cylinder is easier than for the sphere and therefore provides a more direct illustration of the physical mechanism. In this section, we will not include rotation yet, so the floating cylinder is assumed to be at rest. We compute the pressure at the inlet

Fig. 2. A "granite wheel" fountain, in which the levitated object is a cylinder instead of a sphere. The disk in this particular fountain has an estimated radius of $R = 0.50\,m$ and approximate width $0.30\,m$ and is immersed in the fluid to an angle θ_{max} of about $35°$ or $0.60\,rad$ [cf. Fig. 3(a)].

nozzle (or equivalently, the inflow rate Q_{in}) required to give the fluid layer the desired thickness h of a few tenths of a millimeter—sufficiently large for two well-polished surfaces to not grind each other and at the same time sufficiently small to guarantee that no fingers (not even those of the smallest children) can get caught between them.

A. Physical mechanism: Balance of forces

The mechanism of levitation requires an upward force that balances the weight of the levitated object. In the case of a cylinder of radius R and length L, this weight is

$$F_g = \pi R^2 L g \rho_{gr}, \tag{2}$$

where $\rho_{gr} = 2.75 \times 10^3\,kg/m^3$ is the density of granite and $g = 9.81\,m/s^2$ is the gravitational field strength. The net levitation force is provided by the gauge pressure $P(\theta) - P_{atm}$ inside the fluid layer. We anticipate that this pressure is not uniform, but rather a function of the angle θ defined in Fig. 3(a). The associated force then follows from an integral of $[P(\theta) - P_{atm}] \cos \theta$ (the excess pressure on the cylinder, taken in the vertically upward direction) over the submerged surface:

$$F_{up} = \iint_{\mathcal{A}_{sub}} [P(\theta) - P_{atm}] \cos \theta \, dA$$
$$= LR \int_{-\theta_{max}}^{\theta_{max}} [P(\theta) - P_{atm}] \cos \theta \, d\theta. \tag{3}$$

The desired balance between gauge pressure and weight is achieved when $F_{up} = F_g$, or $\int [P(\theta) - P_{atm}] \cos(\theta) \, d\theta = \pi R g \rho_{gr}$. In order to proceed, we thus need to know the gauge pressure $P(\theta) - P_{atm}$ inside the fluid layer.

One may note that, next to the pressure, also the shear stress in the liquid contributes to the force on the cylinder. As the stress τ induces a force parallel to the solid surface, rather than perpendicular as is the case for the pressure, the
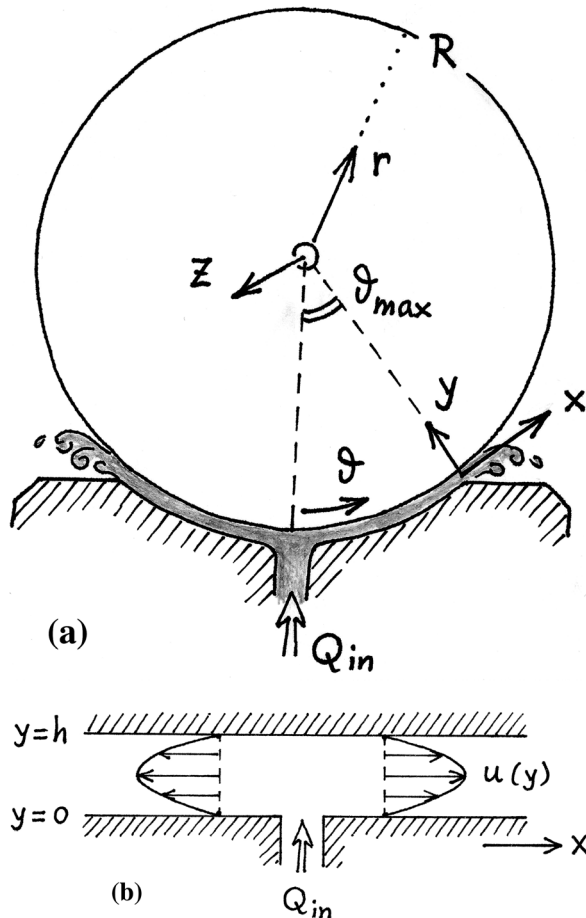
Fig. 3. (a) Sketch of the cylindrical fountain. The gap coordinates (x, y, z) parallel and perpendicular to the curved surface are related to the cylindrical coordinates (r, θ, z) as $x = R\theta$, $y = R + h - r$, and $z = z$, where R denotes the radius of the cylinder and h the thickness of the fluid layer. The cylinder is submerged up to the angle θ_{max}. The thickness of the layer has been greatly exaggerated for the sake of clarity. (b) The flow inside the water layer is essentially straight since $h \ll R$. After leaving the inlet nozzle, the velocity profile $u(y)$ quickly takes a parabolic shape.

contribution to the upward force is of the form $dF_\tau = \tau \sin \theta \, dA$. As we will show, however, the shear stress is much smaller than the pressure (by a factor h/R) and therefore the contribution of the shear stress may be omitted in Eq. (3).

For simplicity, we also omit the contribution from the buoyant force. Given that the depth of the basin is $R(1 - \cos \theta_{max})$ $= 0.175R$ (for $\theta_{max} = 0.60 \, \text{rad}$), only a small part of the cylinder's volume is under water: the submerged fraction is given by $(\theta_{max} - \cos \theta_{max} \sin \theta_{max})/\pi = 0.043$. The associated buoyant force is ρg times the submerged volume $(0.043R^2L\rho g$, with ρ the density of water), which amounts to a fraction $0.043\rho/\rho_{gr} = 0.016$, or 1.6% of the cylinder's weight. A similar calculation for the spherical fountain yields that the submerged volume fraction in that case is $(2 + \cos \theta_{max})$ $(1 - \cos \theta_{max})^2/4 = 0.0069$, meaning that the buoyant force compensates no more than 0.0025 (0.25%) of the kugel's weight. Clearly, the levitation owes little to Archimedes' law of buoyancy.

B. The fluid mechanical equations

The pressure field (and the related velocity field) can be found by solving the set of partial differential equations that express the mass and momentum balance within the fluid. The mass balance is represented by the continuity equation

$$\frac{\partial \rho}{\partial t} + \nabla \cdot (\rho \mathbf{u}) = 0, \tag{4}$$

where ρ is the density of the fluid and $\mathbf{u}$ the velocity field. For an incompressible fluid ($\rho = \text{constant}$) like water this simplifies to $\nabla \cdot \mathbf{u} = 0$. The natural coordinates for the cylindrical fountain are r, θ and z [see Fig. 3(a)], but in view of the fact that the liquid film is extremely thin ($h/R \ll 1$) we may also treat the flow as being essentially along a straight line and use the coordinates (x, y, z) parallel and perpendicular to the surface of the cylinder, as in Fig. 3(b). In principle, the velocity field could have three components $\mathbf{u} = u\mathbf{e}_x$ $+v\mathbf{e}_y + w\mathbf{e}_z$, but due to the symmetry in the z-direction—and ignoring the edges of the cylinder—the velocity in the z-direction may be assumed to be identically zero. In addition, after leaving the nozzle the flow field rapidly orients itself in the x-direction, so the velocity in the y-direction will be zero. Thus, in the steady state we have[5] $\mathbf{u} = u(x, y)\mathbf{e}_x$, independent of z or t. The continuity equation $\nabla \cdot \mathbf{u} = \partial u/\partial x$ $+ \partial v/\partial y + \partial w/\partial z = 0$ then reduces to

$$\frac{\partial u}{\partial x} = 0, \tag{5}$$

from which we infer that the velocity is also independent of x, so that $\mathbf{u} = u(y)\mathbf{e}_x$.

The momentum balance is expressed by the Navier-Stokes equation, which for fluids with constant density ρ and viscosity μ is given by

$$\rho \left[\frac{\partial \mathbf{u}}{\partial t} + (\mathbf{u} \cdot \nabla)\mathbf{u} \right] = \rho \mathbf{g} - \nabla P + \mu \nabla^2 \mathbf{u}. \tag{6}$$

It is the presence of the nonlinear term $(\mathbf{u} \cdot \nabla)\mathbf{u}$ on the left hand side that makes this equation so notoriously difficult to solve in general. Fortunately, in the present case, all terms on the left hand side (proportional to the fluid density ρ) are negligibly small in comparison with the viscous term $\mu \nabla^2 \mathbf{u}$ on the right hand side. This means that inertia of the fluid plays a negligible role, making the cylindrical fountain an example of Stokes (or creeping) flow (a term arising after Stokes' seminal 1851 paper on the subject[6]). Usually, this type of flow is associated with low Reynolds number (Re < 1) but in the present case it also holds for larger values of Re. Indeed, the first term in Eq. (6) vanishes because we consider steady flow ($\rho \partial u/\partial t = 0$) and the second term $\rho(\mathbf{u} \cdot \nabla)\mathbf{u} = \rho u \partial u/\partial x \, \mathbf{e}_x$ is identically zero on account of Eq. (5).

In a more general setting, when the derivative $\partial u/\partial x$ is not equal to zero, inertial effects could come into play. This is, for instance, the case for the spherical fountain. In that case one estimates the relative importance of the fluid inertia by inserting the order-of-magnitude estimates $\partial u/\partial x \sim U/R$ and $\partial^2 u/\partial y^2 \sim U/h^2$ (where U denotes a characteristic value of the velocity). Then, the condition $\rho u \partial u/\partial x \ll \mu \partial^2 u/\partial y^2$ can be written as $\rho U^2/R \ll \mu U/h^2$, or equivalently[7,8]

$$\frac{h^2}{R^2} \left(\frac{\rho UR}{\mu} \right) = \frac{h^2}{R^2} \, \text{Re} \ll 1, \tag{7}$$

where Re $= \rho UR/\mu$ is the Reynolds number based on the kugel radius R. It is at once apparent (even when $\partial u/\partial x$ is

not identically zero) that our analysis need not be restricted to low Reynolds number. Provided the film thickness h is small with respect to the radius of the levitated object ($h \ll R$), the Reynolds number Re based on R may in fact be quite large. This puts our problem into a special class of Stokes flows called *lubrication* flows,[9] first analyzed by Reynolds in 1886.[10] According to Eq. (7), the appropriate dimensionless parameter can be thought of as a Reynolds number based on the length scale h^2/R, which is a subtle combination of the kugel radius and the thickness of the water layer. We note that the cylindrical fountain, with $\partial u/\partial x = 0$, is an exceptionally pure example of lubrication flow.

Returning to Eq. (6), we can see that the gravitational term $\rho \mathbf{g}$ is negligibly small in the problem at hand if we recognize that the effect of gravity is simply to add a hydrostatic component to the pressure. With $\rho = 10^3 \, \text{kg/m}^3$ and an estimated film thickness of $h = 0.3 \, \text{mm}$, the magnitude of this gravitational contribution to the fluid pressure is at most $\rho g h \approx 3 \, \text{Pa} = 3 \times 10^{-5} \, \text{atm}$. Comparing this to the required gauge pressure at the inlet nozzle (which is in the order of several tenths of an atmosphere) we see that the contribution from gravity is indeed marginal and may safely be neglected. The Navier-Stokes equation then reduces to

$$0 = -\nabla P + \mu \nabla^2 \mathbf{u}, \tag{8}$$

which is known as the "Stokes flow" or "creeping flow" approximation.[7,8,11,12] The components of this equation represent a balance of pressure and viscous stress inside the fluid layer. Inertia of the fluid (represented by the fluid density ρ) plays no role for the cylindrical fountain.

C. Pressure field and velocity inside the fluid layer

Solving the creeping flow equation—The problem is now properly laid out and we are ready to solve for the flow and pressure inside the fluid layer. With the fluid speed $u(y)$ depending only on the perpendicular position within the layer, the components of Eq. (8) take the form

$$\frac{\partial P}{\partial x} = \mu \frac{d^2 u}{dy^2}, \tag{9}$$

$$\frac{\partial P}{\partial y} = 0, \tag{10}$$

$$\frac{\partial P}{\partial z} = 0. \tag{11}$$

The latter two equations imply that the pressure is a function of x only; the first equation can then be solved by separation of variables. Recognizing that the expression on the left-hand side does not depend on y while the right-hand side does not depend on x, the only consistent solution is that *both* sides depend neither on x nor y but are simply constant. For reasons that will become clear in a moment, this constant has to be negative, say $-\mu K$, and thus Eq. (9) yields

$$\frac{dP}{dx} = \frac{1}{R}\frac{dP}{d\theta} = -\mu K \tag{12}$$

and

$$\frac{d^2 u}{dy^2} = -K. \tag{13}$$

The first of these two equations immediately reveals the reason why the constant $(-\mu K)$ had to be negative: the pressure must decrease from the inlet nozzle to the rim of the socket so the pressure gradient $dP/d\theta$ must necessarily be negative. Integrating Eq. (12) yields the form of the pressure profile

$$P(\theta) = P(0) - \mu R K \theta, \tag{14}$$

where $P(0)$ is the pressure at the inlet nozzle. The pressure at θ_{max} where the flow meets the surrounding air must be P_{atm} (=1 atm), so $P_{\text{atm}} = P(0) - \mu R K \theta_{\text{max}}$. This gives the gauge pressure $P(0) - P_{\text{atm}} = \mu R K \theta_{\text{max}}$. The only unknown in this relation, K, will follow when we solve Eq. (13).

Integrating Eq. (13), we find that the velocity profile has the form $u(y) = A + By - (1/2)Ky^2$, where A and B are integration constants to be determined from the boundary conditions. We employ no-slip boundary conditions at the socket ($y = 0$) and at the surface of the cylinder ($y = h$). If the cylinder is not rotating this means that the speed vanishes at both boundaries, giving respectively $A = 0$ and $B = (1/2)Kh$, hence we arrive at the parabolic velocity profile [see also Fig. 3(b)]

$$u_0(y) = \frac{1}{2} \, Ky(h - y), \tag{15}$$

where we use the subscript "0" to indicate zero rotation. This is the well-known planar *Poiseuille* velocity profile for flow between parallel plates under the influence of a constant pressure gradient. The constant K sets the strength of the velocity field and is directly related, as we shall see, to the fluid influx Q_{in} at the nozzle.

Mass balance—The inflow rate Q_{in} has dimensions of volume per unit time (e.g., liters per minute) and is, in the absence of rotation, equally distributed over the left and right sides of the cylinder. By mass conservation, this must be equal to the flow integrated across the fluid layer

$$\frac{Q_{\text{in}}}{2} = L \int_0^h u_0(y) \, dy = \frac{1}{12} L K h^3, \tag{16}$$

where we have simply integrated the velocity profile (15). So the constant K is found to be

$$K = \frac{6 Q_{\text{in}}}{L h^3}, \tag{17}$$

which is, as expected, directly proportional to the inflow rate.

Pressure field—With the above value of K, the value of the gauge pressure at the inlet nozzle becomes

$$P(0) - P_{\text{atm}} = \mu R K \theta_{\text{max}} = \frac{6 \mu R Q_{\text{in}}}{L h^3} \theta_{\text{max}} \tag{18}$$

and $P(\theta)$ for every angle between 0 and θ_{max} is then readily obtained using Eq. (14):

$$P(\theta) - P_{\text{atm}} = \frac{6 \mu Q_{\text{in}} R}{L h^3} (\theta_{\text{max}} - |\theta|). \tag{19}$$

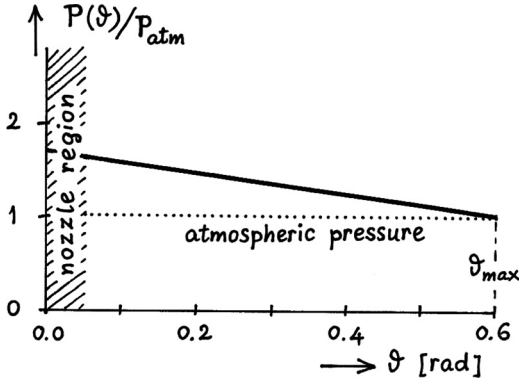The pressure field $P(\theta)$ is shown in Fig. 4 for typical parameter values (see Sec. II D); it is symmetric around the flow

Fig. 4. The linear pressure distribution $P(\theta)/P_{atm}$ in the water layer under the levitated cylinder, given by Eq. (19). The radius and width of the cylinder are taken to be $R = 0.50$ m and $L = 0.30$ m, mimicking the granite wheel of Fig. 2, and the inflow rate is $Q_{in} = 0.30$ L/s. The associated thickness of the fluid layer is 0.29 mm [cf. Eq. (21)]. Above and close to the inlet nozzle (from $\theta = 0$ to about $\theta \approx 0.05$ rad) the pressure field may be expected to deviate from the straight line; that is why this part of the plot has been hatched. The outer rim of the fountain, where the water meets the air and hence the fluid pressure equals the atmospheric pressure, lies at $\theta = \theta_{max} = 0.60$ rad ($\approx 35°$).

inlet ($\theta = 0$) and decreases with a constant negative gradient ($-\mu R K$) until it reaches P_{atm} at the edge of the socket at θ_{max}.

The strong h-dependence of the pressure, $P \sim \mu Q_{in} R/L h^3$, is one of the foremost features of lubrication flow. If we compare P to the typical shear stress at the kugel surface, $\tau = \mu du/dy \sim \mu Q_{in}/L h^2$, we find that $\tau/P \sim h/R \ll 1$. The smallness of this ratio is the origin of the renowned low friction in lubrication layers. Without the lubricant, Coulomb's friction law would dictate the frictional force (shear stress × area) to be equal to the friction coefficient f times the normal force (pressure × area), so in that case the ratio τ/P would be $f \approx 0.6$ (for granite on granite).

D. Thickness of the fluid layer

Now that we know $P(\theta) - P_{atm}$ in terms of μ and Q_{in}, we are in a position to compute the integral in Eq. (3) to obtain the net levitation force. The result is

$$F_{up} = \frac{12\mu Q_{in} R^2}{h^3}(1 - \cos\theta_{max}). \tag{20}$$

In equilibrium, this upward force is equal to the weight of the cylinder F_g, Eq. (2), and thus we arrive at the expression for the film thickness:

$$h = h_{cyl} = \left[\frac{12}{\pi}(1 - \cos\theta_{max})\right]^{1/3}\left(\frac{\mu Q_{in}}{L g \rho_{gr}}\right)^{1/3}. \tag{21}$$

The subscript "cyl" indicates that this result concerns the cylindrical fountain. The inlet of the cylindrical fountain is not point-like, but rather distributed along a line of length L, and Q_{in}/L represents the inflow rate per unit length along this line. For clarity, the expression (21) has been split into a dimensionless prefactor (depending on the geometry of the fountain via θ_{max}) and a factor that has the dimension of a length. Interestingly, in the case of the cylindrical fountain, the thickness of the fluid layer is independent of the radius R of the cylinder. The physical explanation for this is that both

the levitation force and the weight of the cylinder scale as R^2 and thus cancel in the end result for h.

To get a feel for Eq. (21), let us insert typical values of the fountain parameters, taking the granite wheel in Fig. 2 as an example. From the figure, we estimate that θ_{max} is a little under $35°$ (or 0.60 rad), giving a prefactor of 0.87. With $L \approx 0.30$ m, the density of the wheel $\rho_{gr} = 2.75 \times 10^3$ kg/m³, the viscosity of water $\mu = 1.00 \times 10^{-3}$ Pa·s, and a typical inflow rate Q_{in} of 0.30 liters per second (0.30×10^{-3} m³/s) we arrive at a film thickness of $0.87(\mu Q_{in}/\rho g L)^{1/3} \sim 0.3$ mm. This is satisfactorily small: there is no danger for fingers being caught between the wheel and the socket. The small value of h also justifies our earlier assumption that $h/R \ll 1$. In the present example, this ratio is $h/R = 0.6 \times 10^{-3}$, which is very good news in the context of the lubrication condition Eq. (7).

In practice, it is wise to choose the inflow rate such that the film thickness is several tenths of a millimeter. We note, however, that there is no specific threshold value of Q_{in} below which the fountain would not work in principle. As long as Q_{in} is positive, the pressure $P(0)$ at the inlet will always exceed the atmospheric pressure and a thin lubrication layer establishes itself between the basin of the fountain and the cylinder. If the surfaces were perfectly smooth, any supramolecular thickness h (corresponding to tiny inflow rates Q_{in}) would be sufficient to make the fountain work. The only problem with choosing a very small value of Q_{in} is that it will render the system rather vulnerable; small irregularities in the masonry, a slight unbalance, or even sand grains caught in the fluid layer may be enough to cause scratches on the polished surfaces.

III. SPHERICAL FOUNTAIN

We now turn to the spherical fountain. In Fig. 5, we show the kugel fountain that adorns the main entrance of the House of Science in Patras, Greece, where we were allowed to perform some elementary measurements. The granite sphere has a diameter of precisely one meter ($R = 0.50$ m) and, by trying to fit plastic sheets of different thickness inside the gap between the sphere and the socket, we found that the thickness of the water layer is $h = 0.30 \pm 0.05$ mm. In this section, we will show that such a thickness is indeed

Fig. 5. The kugel fountain at the House of Science in Patras, Greece. The granite sphere has a diameter of precisely 1 m and is immersed in the water basin up to an angle $\theta_{max} \approx 35°$. We measured the thickness of the water layer to be 0.30 ± 0.05 mm.

consistent with hydrodynamic theory. For sufficiently small inflow rates the calculation can again be based on Stokes flow alone, i.e., neglecting the liquid inertia. At higher flow rates, however, inertial effects become increasingly important for the spherical fountain and this turns out to have a negative effect on the levitation force. Consequently, Q_{in} should neither be too small (as before, to avoid scratches) nor too large (to prevent the inertial effects from becoming dominant), meaning that there exists some intermediate range of Q_{in} for which the fountain works optimally.

A. Creeping flow approximation

The spherical fountain calls for a three-dimensional analysis (see Fig. 6). The flow is now radially outward from the inlet nozzle so that $\mathbf{u} = (u_r, u_\theta, u_\phi) = u_0(r, \theta)\,\mathbf{e}_\theta$, and as the fluid is being spread over a region of increasing area its speed must decrease with θ to ensure conservation of mass. (This deceleration means that the inertial term $\rho(\mathbf{u} \cdot \nabla)\mathbf{u}$ in the Navier-Stokes equation is not identically zero anymore, but for the time being we shall assume it is still small in comparison with the terms ∇P and $\mu \nabla^2 \mathbf{u}$, which is a valid approximation as long as the inflow rate Q_{in} is sufficiently small.) When reaching an angle θ, the circumference of the cross-section has become $2\pi R \sin \theta$, and the total flux through this circumference per unit time is simply

$$Q_{in} = 2\pi R \sin \theta \int_0^h u_0(y, \theta)\, dy. \tag{22}$$

Once more, the velocity profile across the fluid layer is parabolic in the creeping flow approximation. So we set $u_0(y, \theta) = (1/2)K(\theta)y(h - y)$ and the integral in Eq. (22) is then readily evaluated to give

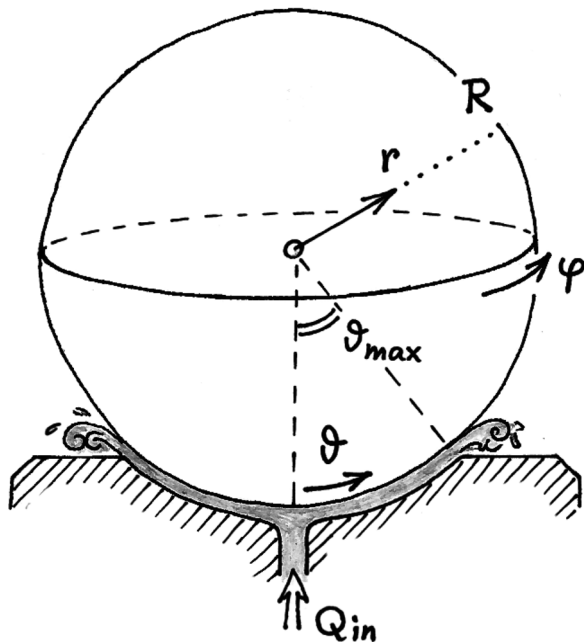$$Q_{in} = \frac{1}{6}\pi R \sin \theta\, K(\theta) h^3, \tag{23}$$

showing that the factor $K(\theta)$ in the expression for the velocity decreases as $1/\sin\theta$:

$$K(\theta) = \frac{6Q_{in}}{\pi R h^3 \sin \theta}, \tag{24}$$

and hence

$$u_0(y, \theta) = 3\left(\frac{Q_{in}}{\pi R h^3}\right)\frac{y(h - y)}{\sin \theta}. \tag{25}$$

We proceed along the same lines as for the cylindrical fountain, picking up the analysis at Eqs. (12) and (13). The relation (13) corresponds to the above assumption of a parabolic velocity field. With the factor K being given by Eq. (24), the gauge pressure $P(\theta) - P_{atm}$ can then be computed from the equation for the pressure gradient (12):

$$P(\theta) - P_{atm} = \frac{6\mu Q_{in}}{\pi h^3}\,\ln\left[\frac{(1 - \cos\theta_{max})\sin\theta}{(1 - \cos\theta)\sin\theta_{max}}\right]. \tag{26}$$

This pressure profile is depicted in Fig. 7 (solid curve). Interestingly, the pressure exhibits a singularity at $\theta = 0$, where the logarithmic factor diverges (this can be traced back to the diverging velocity $\sim 1/\sin\theta$). This poses no problem, however. In the first place, we should exclude the immediate neighborhood of the nozzle—a small area around $\theta = 0$—because our analysis does not cover this region (the velocity of course does not diverge in reality). Secondly, even if we choose to use the above expression for the pressure down to $\theta = 0$, the contribution to the levitation force remains finite:
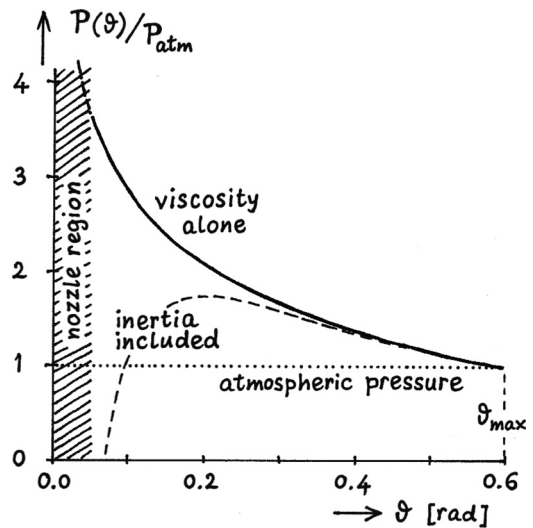

Fig. 6. The spherical coordinates (r, θ, ϕ) for the kugel fountain. Within the fluid layer one may also conveniently use the coordinates (x, y, ϕ), with $x = R\theta$ and $y = R + h - r$ as in Fig. 3. The thickness of the fluid layer has been exaggerated for clarity.

Fig. 7. Pressure distribution $P(\theta)/P_{atm}$ under the spherical fountain of Fig. 5. The solid curve is the pressure due to viscosity alone, given by Eq. (26), while the dashed curve includes also the contribution from the inertial effects [Eq. (31)]. We take a typical water influx of $Q_{in} = 1.5\,\text{L/s}$, and the associated thickness of the fluid layer is 0.31 mm. The hatched area indicates the nozzle region (from $\theta = 0$ to $\theta \approx 0.05$ rad) where the water flows into the system and the actual pressure will deviate from our theory; thus, both the logarithmic singularity in the solid curve for $\theta \to 0$, as well as the strong Bernoulli suction when the dashed curves dives to negative values, are shrouded and made harmless by the presence of the nozzle. The outer rim of the fountain, where the water meets the air (and hence the fluid pressure becomes equal to the atmospheric pressure), lies at $\theta = \theta_{max} = 0.60$ rad.

$$F_{\mathrm{up}} = \iint_{\mathcal{A}} [P(\theta) - P_{\mathrm{atm}}] \cos \theta \, dA$$

$$= \int_0^{2\pi} \int_0^{\theta_{\max}} [P(\theta) - P_{\mathrm{atm}}] \cos \theta \, R^2 \sin \theta \, d\theta \, d\phi$$

$$= \frac{6\mu Q_{\mathrm{in}} R^2}{h^3} (1 - \cos \theta_{\max}). \tag{27}$$

So we see that the logarithmic singularity in the pressure is tamed by the smallness of the area around the origin over which it is integrated.

Now, by equating the above levitation force [Eq. (27)] to the weight of the sphere, $F_g = (4/3)\pi R^3 g \rho_{\mathrm{gr}}$, one readily obtains the thickness of the fluid layer for the spherical fountain (in the creeping flow approximation)

$$h_{\mathrm{sph}} = \left[\frac{9}{2\pi} (1 - \cos \theta_{\max}) \right]^{1/3} \left(\frac{\mu Q_{\mathrm{in}}}{R g \rho_{\mathrm{gr}}} \right)^{1/3}. \tag{28}$$

This result for the spherical fountain has essentially the same structure as that for the cylindrical fountain [see Eq. (21)] and illustrates that a perfectly polished spherical fountain (just like the cylindrical one) does not require a specific threshold value of Q_{in} in order to function. As long as Q_{in} is positive, small as it may be, a lubrication layer with a finite thickness h will establish itself.

Taking the fountain depicted in Fig. 5 as an example (with $R = 0.50$ m, $\theta_{\max} = 0.6$ rad, $\mu = 10^{-3}$ Pa · s, $\rho_{\mathrm{gr}} = 2750$ kg/m^3) and setting the inflow rate to $Q_{\mathrm{in}} = 0.3$ L/s $= 0.3 \times 10^{-3}$ m^3/s, Eq. (28) yields a value for the gap width of $h_{\mathrm{sph}} \approx 0.18$ mm. A smoothly polished kugel may just be able to operate with such a thin water layer. To be on the safe side, however, it is good to have a somewhat thicker layer and this can readily be accomplished by choosing a larger inflow rate. At $Q_{\mathrm{in}} = 1.5$ L/s, Eq. (28) predicts a layer thickness $h_{\mathrm{sph}} = 0.31$ mm, in excellent agreement with the 0.30 ± 0.05 mm, we measured on the fountain of Fig. 5.

B. Inertial effects: Bernoulli suction

Contrarily to the cylindrical fountain, the velocity in the film below the sphere is not uniform, but decreases as $1/\sin\theta$. This means that the inertia of the liquid can become important: the deceleration of the fluid mass induces an extra contribution to the pressure field inside the water layer, originating from the advection term $\rho(\mathbf{u} \cdot \nabla)\mathbf{u}$ in Eq. (6). To estimate the importance of this advection term with respect to the viscous term $\mu \nabla^2 \mathbf{u}$, we check whether the condition (7) is still satisfied. For the parameter values cited above (with $Q_{\mathrm{in}} = 1.5$ L/s) the Reynolds number is Re $= \rho U R / \mu \sim 10^6$. Given that $(h/R)^2 \sim 10^{-6}$ we must conclude that $(h/R)^2$Re is of order unity, so inertial effects cannot really be neglected at these values of Q_{in}. As an aside, we note that the Reynolds number based on the film thickness—Re$_h = \rho U h / \mu$—is, for the same value of Q_{in}, still small enough for the flow to remain laminar.

1. Inviscid flow: The yarn spool effect

To illustrate the effect of inertia in its purest form, we first consider the idealized case of inviscid flow. This is the opposite limit of creeping Stokes flow: one now assumes that the inertia (or kinetic energy) of the liquid is so large that it

completely dominates over viscous friction. If in addition the flow is steady and irrotational, one can integrate the Navier-Stokes equation (6) to a very simple form: $\frac{1}{2}\rho|\mathbf{u}|^2 + \rho g y + P =$ constant, or if we neglect gravity as before,

$$\frac{1}{2}\rho|\mathbf{u}|^2 + P = C, \tag{29}$$

where C is a constant. This is the celebrated Bernoulli's law that expresses the conservation of energy in an inviscid flow; regions of high kinetic energy correspond to low pressure, and vice versa. This behavior has a remarkable consequence for the spherical fountain, where mass conservation dictates that the velocity in the water below the sphere decreases from the nozzle to the outlet. According to Bernoulli's law (29), the pressure P is *lowest* at the nozzle. Thus, if it were for the inertial contribution alone, the pressure would in fact be below atmospheric pressure everywhere except at the outer rim. Rather than providing a levitating force, the inertial pressure induces a downward force that attracts the sphere towards the socket. This effect is known as *Bernoulli suction*.

A classic demonstration of Bernoulli suction is the experiment with a paper card and a spool illustrated in Fig. 8. When air is blown through the spool, the increased air velocity in the layer between the spool and the card means (according to Bernoulli's law) that a region of low pressure is created here. As a result, the atmospheric pressure of the ambient air pushes the card against the spool.

If $u(r)$ denotes the radially outward velocity in the layer at a distance r from the inlet, and $P(r)$ the local pressure, Bernoulli's law tells us that $(1/2)\rho u^2(r) + P(r) = (1/2)\rho u^2(r_{\max}) + P_{\mathrm{atm}}$, with $r_{\max}$ the radius at the rim where the layer meets the ambient atmosphere. Now, by mass conservation $Q_{\mathrm{in}} = 2\pi r u(r) h$, or $u(r) = Q_{\mathrm{in}}/(2\pi h r)$, and thus we get

$$P(r) = P_{\mathrm{atm}} - \frac{1}{2}\rho \left[u^2(r) - u^2(r_{\max}) \right]$$

$$= P_{\mathrm{atm}} - \frac{\rho Q_{in}^2}{8\pi^2 h^2} \left(\frac{1}{r^2} - \frac{1}{r_{\max}^2} \right). \tag{30}$$
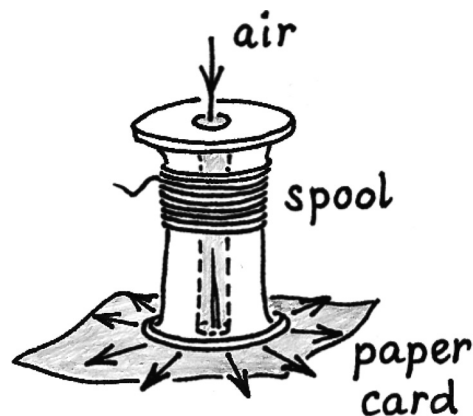

Fig. 8. The classic demonstration of Bernoulli suction, using a spool and a paper card with a thin needle pierced through it to keep it centered with respect to the hole of the spool. If one blows air through the spool, the increased air velocity in the narrow layer between the spool and the card induces (by Bernoulli's law) a region of low pressure. As a result, the atmospheric pressure of the ambient air pushes the card against the spool. The demonstration is usually done upside down, as in the above picture, to show that (apart from the surprising fact that the card is not simply blown away) the Bernoulli suction can even defy gravity.

Clearly, the pressure in the layer is everywhere smaller than P_{atm}; it only attains this value at $r = r_{max}$.

2. Inertial effects and the granite sphere fountain

From the above analysis, it is evident that the granite sphere can only be levitated when viscosity dominates over inertia. If not, the pressure reduction due to the decelerating liquid would disable the fountain. This means that one should not make the inflow rate too large (because the relative influence of inertia grows with Q_{in}). On the other hand, as we have noted before, one should not make Q_{in} too small in order to avoid damaging contact between the kugel and the basin. Hence, there is an *intermediate* range of Q_{in} for which the spherical fountain works optimally.

A consistent description that includes both viscous and inertial effects is notoriously difficult for the Navier-Stokes equations. This is why we have until now concentrated on the limiting cases of purely viscous and purely inertial flow. If one wants to combine the two, one generally has to reside to approximation schemes. For a radial flow between two parallel discs in the horizontal plane (such as the spool of Fig. 8 and arguably also the spherical fountain, since the curvature of the kugel plays only a minor role), this problem has recently been addressed by Armengol *et al.* in this journal.[13] They derive the following approximate expression for the pressure field in the fluid layer:

$$P(r) = P_{atm} + \frac{6\mu Q_{in}}{\pi h^3} \ln\left(\frac{r_{max}}{r}\right) - \frac{27\rho Q_{in}^2}{140\pi^2 h^2}\left(\frac{1}{r^2} - \frac{1}{r_{max}^2}\right). \tag{31}$$

In this equation, one recognizes the pressure contributions from viscosity and inertia, respectively; their structure is very similar to the previously derived exact expressions (26) and (30) for the idealized limiting cases. As expected, the pressure due to viscosity generates a positive levitating force whereas the inertial pressure works in the negative direction.

We note that the magnitudes of both contributions increase with the inflow rate, but while the viscous pressure grows linearly with Q_{in}, the inertial contribution scales as Q_{in}^2. This confirms our earlier observation that the dominance shifts from the viscous to the inertial regime as Q_{in} is gradually increased. Using the estimates $Q_{in} \sim hRU$ and $r \sim R$, one verifies from Eq. (31) that the cross-over takes place when $\rho U h^2/(\mu R)$ is of order unity, consistent with Eq. (7). Eventually, at large flow rates, the generated levitating force will no longer be able to lift the kugel. In Fig. 7, we have sketched how inertial effects change the pressure profile in the fluid layer below the granite sphere (dashed curve).

IV. DAMPING OF ROTATIONS

Anybody who has ever put his or her hands on the kugel fountain will have experienced that the sphere is easily set into a rotating motion and that it takes a surprisingly long time before the sphere comes to a halt. This is because there is no direct contact between the sphere and the socket, making friction very low. In fact, the only source of friction lies in the viscous drag the fluid layer exerts on the sphere and this is exactly the same principle on which roller bearings work. In this section, we compute this small viscous drag

and show that it causes the angular speed to slow down exponentially as $\omega(t) = \omega(0)\exp(-t/t_{rel})$, with a relaxation time t_{rel} of the order of 10 min. We first address the cylindrical fountain, which we treat analytically, and then present experimental results for the case of a sphere.

A. The cylindrical fountain: Analysis

When the cylinder is set into rotation with angular frequency ω, the velocity at the cylinder surface becomes $u = R\omega$. This has an effect on the flow inside the water layer. The no-slip boundary condition now becomes $u(y = h) = \omega R$. As illustrated in Fig. 9, the resulting profile can be seen as a superposition of the *Poiseuille* parabolic profile and a simple linear *Couette* profile. Such a superposition is allowed since the Stokes equation (8) is linear with respect to the velocity. Mathematically, the profile can thus be written as $u(y) = u_0(y) + u_\omega(y)$, where $u_0(y)$ is the profile without rotation, given by Eq. (15), and

$$u_\omega(y) = \omega R \frac{y}{h}. \tag{32}$$

Interestingly, the rotational profile has zero second derivative ($d^2 u_\omega/dy^2 = 0$) and therefore does not contribute to the pressure balance $\partial P/\partial x = \mu d^2 u/dy^2 = \mu d^2 u_0/dy^2$, cf. Eq. (9). So the pressure distribution $P(\theta)$ is unaffected by rotation.

The main effect of the rotation is to break the left-right symmetry of the system and hence it produces a nonzero frictional torque (i.e., force moment) on the cylinder. The cylinder applies a force on the water and, by Newton's third law, the water applies an equally strong reaction force on the cylinder. This is accomplished via the shear stress τ in the water layer, which can be computed as

$$\tau = \tau_0 + \tau_\omega = \mu\left(\frac{du_0}{dy} + \frac{du_\omega}{dy}\right). \tag{33}$$

Shear stress is also present when there is no rotation but by symmetry the Poiseuille contribution τ_0 does not yield a net torque on the cylinder; the entire net torque comes from the Couette contribution $\tau_\omega = \mu R\omega/h$. We can compute the torque on the cylinder by integrating the force moment $dT = -R\tau_\omega dA$ over the submerged surface

$$\begin{aligned} T &= -\iint_{\mathcal{A}} R\tau_\omega \ dA \\ &= -\int_{-\theta_{max}}^{\theta_{max}} R\frac{\mu R\omega}{h} \ LR \ d\theta \\ &= -\frac{2\theta_{max}\mu L R^3}{h} \ \omega. \end{aligned} \tag{34}$$

The frictional torque is thus proportional to ω and opposite to the direction of rotation. It will slow down the rotation according to the equation of motion

$$T = I_{cyl}\frac{d\omega}{dt}, \tag{35}$$

where $I_{cyl} = (1/2)MR^2 = (1/2)\rho_{gr}\pi L R^4$ is the moment of inertia of the granite wheel. Given the expression for T above, this equation of motion takes the form
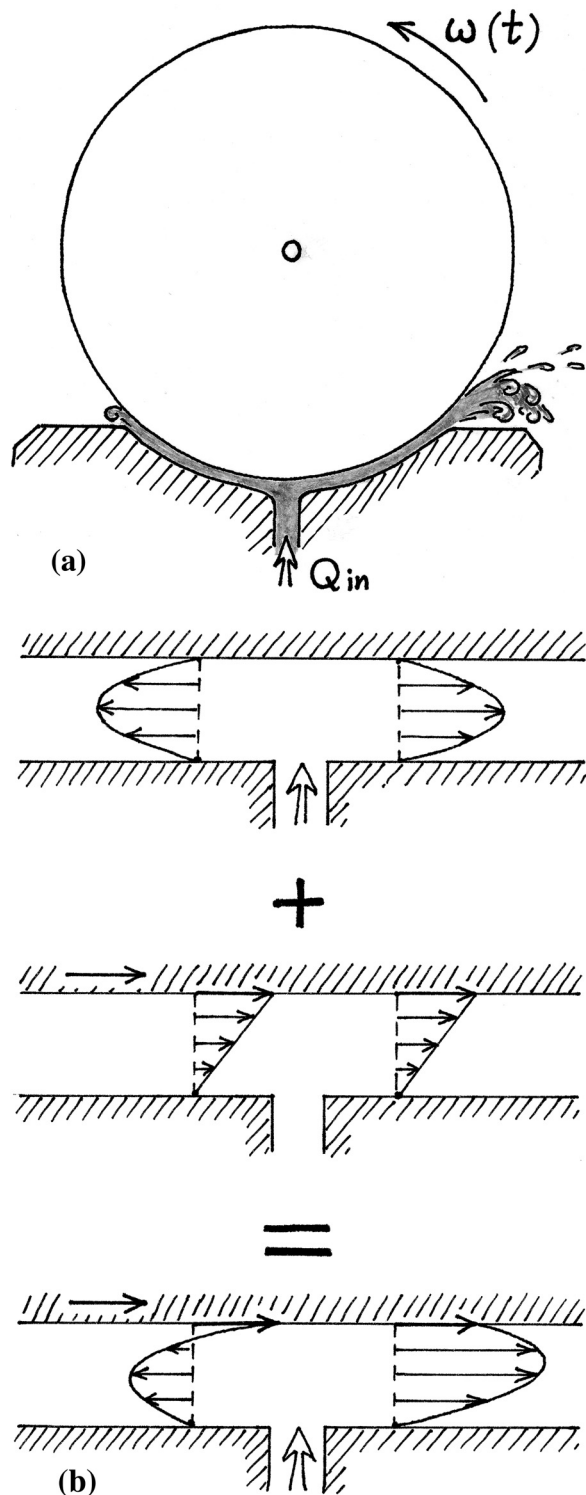
(a)

Q_{in}

(b)

Fig. 9. (a) Rotation of the levitated object breaks the symmetry of the flow inside the fluid layer. (b) The velocity field is now a superposition of the parabolic Poiseuille profile (caused by the pressure gradient from the inlet nozzle to the surrounding air) and the linear Couette profile caused by the velocity difference between the socket, which is at rest, and the surface of the kugel moving at speed ωR.

$$\frac{d\omega}{dt} = -\frac{4\theta_{max}\mu}{\pi\rho_{gr}Rh}\omega, \tag{36}$$

which is easily solved to give an exponential decay

$$\omega(t) = \omega_0 e^{-t/t_{rel}}, \tag{37}$$

with the relaxation time t_{rel} given by

$$t_{rel} = \frac{\pi}{4\theta_{max}}\frac{\rho_{gr}Rh}{\mu}. \tag{38}$$

This relaxation time consists of a characteristic time scale for the damping, $\rho_{gr}Rh/\mu$, multiplied by a dimensionless geometric prefactor. Using the same fountain parameters as in Sec. II ($\rho_{gr} = 2750\,\text{kg/m}^3$, $R = 0.5\,\text{m}$, $h = 0.3\,\text{mm}$, $\theta_{max} = 0.6\,\text{rad}$, and $\mu = 0.001\,\text{Pa}\cdot\text{s}$) the characteristic time scale is $\rho_{gr}Rh/\mu = 412\,\text{s}$. Putting in the geometric prefactor, the relaxation time is found to be $540\,\text{s}$, i.e., no less than 9 min! Indeed, the damping of the rotations turns out to be a slow process, with the weak viscous drag only very gradually wearing down the angular momentum of the massive granite wheel.

B. The spherical fountain: Scaling argument and experiment

The calculation of the torque on the sphere is much more involved than for the cylinder. To begin with, the axis of rotation is no longer fixed. There are two basic modes of rotation: around the horizontal axis, as for the cylinder, and also around the vertical axis. The effectiveness of the viscous drag is different for the two modes, due to the fact that the fluid velocity (and thus the strength of the drag) as well as the effective "moment arm" are not uniform over the surface. Rather than pursuing a detailed analysis of the rotating sphere it is more insightful to give a scaling argument that focuses on the essential physics.

In analogy to the torque on the cylindrical wheel, given by Eq. (34), we find for the sphere

$$T \sim \frac{\mu R^4\omega}{h}. \tag{39}$$

Here, the width of the wheel L appearing in Eq. (34) has been replaced by R. Different modes of rotation will have different (geometric) prefactors, but these are not captured by a scaling analysis. The above torque T must be equated to $Id\omega/dt$, where the moment of inertia $I \sim MR^2 \sim \rho_{gr}R^5$, giving

$$\frac{\mu R^4\omega}{h} \sim \rho_{gr}R^5\frac{d\omega}{dt}. \tag{40}$$

Hence, we recover a similar exponential decay of the angular velocity ω as in Eq. (36), with a relaxation time that once more reads

$$t_{rel} \sim \frac{\rho_{gr}Rh}{\mu}. \tag{41}$$

To verify this scaling argument, we have performed a series of experiments on the granite sphere fountain of Fig. 5. Bringing the sphere in a rotation around the horizontal axis, we monitored the decay of the angular velocity during approximately 40 revolutions. By tracking a distinct spot on the surface of the sphere, we were able to determine the time for each complete revolution and thus the angular velocity $\omega(t)$. The results are presented in Fig. 10, showing $\ln\omega$ versus time. The data are seen to lie on a straight line, in excellent agreement with the predicted exponential decay of $\omega(t)$. The slope of the
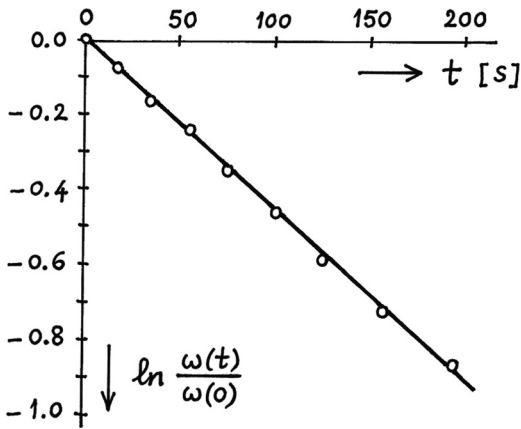
Fig. 10. Measured decrease of the angular velocity $\omega(t)$ for the spherical fountain of Fig. 5 rotating around a horizontal axis. At the start of the experiment, the kugel was given a spinning motion with $\omega(0) = 1.57$ rad/s, i.e., one complete revolution in precisely 4 s. The plot shows that $\ln[\omega(t)/\omega(0)] = -Ct$ with $C = 4.55 \times 10^{-3}$ s^{-1}, or equivalently, that the angular velocity decays exponentially as $\omega(t) = \omega(0)e^{-Ct}$; the corresponding relaxation time is $t_{\mathrm{rel}} = 1/C = 220$ s.

curve can be identified with $-1/t_{\mathrm{rel}}$ and yields $t_{\mathrm{rel}} \approx 220$ s. (The same value was found, within about 15 s, for different runs of the experiment). This value of t_{rel} is consistent with the order-of-magnitude estimate given in Eq. (41), which, for the sphere in question (with $\rho_{\mathrm{gr}} = 2750$ kg/m^3, $R = 0.50$ m, $h = 0.3$ mm and $\mu = 0.001$ Pa $\cdot$ s), predicts a relaxation time of the order of 400 s.

In the above discussion, we have left out several effects that might influence the relaxation time. For one, we expect the inlet nozzle is not positioned precisely in the center of the socket but several centimeters off center. This induces a spontaneous rotation even in the absence of any human intervention, adding a realistic effect to kugels decorated with a map of the Earth and keeping the whole surface properly wetted, and, in all likelihood, affecting the relaxation time. Another feature that has not been taken into account is that the rotation generates an asymmetry in the outflow at the edge of the socket, as sketched in Fig. 9(a): the water comes out with much more vigor on one side (in the direction of the rotation) than on the other. Any extra source of dissipation this asymmetry introduces is beyond the scope of the present analysis.

V. DISCUSSION

In conclusion, we are now in a position to give a definitive answer to our original question, "What makes the fountain work?" It is not Archimedes' law of buoyancy, the favorite of the Science Museum visitors. Instead, it is another basic principle, less familiar to the general public but of key importance in almost every type of machinery: lubrication.

As a matter of fact, the kugel fountain can be thought of as a giant ball bearing. The pressure inside the thin fluid layer (thickness h) scales as $1/h^3$ and is perfectly able to carry the heavy granite sphere. For a given flow rate Q_{in}, usually around 1 L/s, the water layer automatically adjusts itself to the thickness required to lift the weight. The water acts as a lubricant and is responsible for the surprisingly low friction experienced by the sphere.

Another phenomenon that relies on the same lubrication principle is the Leidenfrost drop, shown in Fig. 11. This is a water drop hovering above a hot plate (typically around 250 °C) without touching it, carried by its own vapor
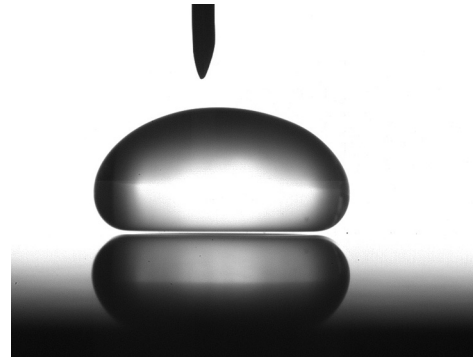

Fig. 11. The Leidenfrost phenomenon: a water drop hovering above a hot plate, levitated by its own thin vapor layer. The horizontal diameter of the drop is about 1 cm. In the upper part of the photo we see the pipette from which the drop was released. Image courtesy of Raphaële Thévenin and Dan Soto.

layer.[14,15] The fact that air is a poor conductor of heat ensures that the drop, instead of instantly boiling away, only slowly evaporates and can survive for more than a minute. The same effect is observed when pouring liquid nitrogen on a table. Nitrogen drops skate freely over the surface with negligible friction, thanks to the lubricating layer of nitrogen vapor. In addition, the popular game of air hockey works on the same principle, only in this case the puck does not evaporate of course, but the lubrication layer is provided by air flowing out of tiny pores in the table.[12]

In all of these examples, the thickness of the layer adjusts itself such that the integrated pressure exactly balances the weight of the levitated object. Owing to the smallness of the gap, the viscous forces inside the flow dominate over the inertial ones. This is, as we have shown, a necessary condition for achieving an upward levitation force. In the above examples, one may wonder whether the compressibility of the air does not fundamentally change the physics of levitation. The effects of compressibility, however, only begin to play a role when the Mach number becomes of order unity. This number is defined as $\mathrm{Ma} = u/c$, where u is the velocity of the flow and c the speed of sound in air. Since the latter is roughly 330 m/s, the Mach number in all examples mentioned remains much smaller than 1, and hence the flow may safely be treated as incompressible.

In fact, the granite sphere fountain itself can operate on air. As compared to water, both viscosity and inertial effects become smaller in air but not to the same degree. While the viscosity μ is reduced by a factor of 50, the density ρ is reduced by no less than a factor of 1000. This means that the troublesome inertial effects are relatively smaller for the air-borne kugel than for the water version, at least as long as we may keep the air inflow rate Q_{in} at a reasonably low level. (Recall that the viscous effects grow linearly with Q_{in}, whereas the inertial effects grow quadratically.) The condition that Q_{in} be kept small poses just one practical challenge: it implies, by Eq. (28), that the gap width h will be very small (typically of the order of 0.30 mm$/50^{1/3} = 0.08$ mm), which calls for a sphere and basin that are both perfectly spherical and exceptionally well polished. The successful lubrication of the kugel with air thus relies, not on a strong airflow, but on the craftsmanship of the stonemason. Not without reason an airborne kugel (a perfectly polished black granite sphere with a diameter of 0.40 m) was awarded a special prize at the International Granite and Stone Fair "Stona 2004" in Bangalore, India.[16]

[1] See the information on various websites, for instance, that of Clute's Kugel in the State Botanical Garden of Georgia in Athens, Georgia at <http://clutebarrow.org/kugel.html>.

[2] From the brochure by Kusser Aicha Granitwerke on *Floating sphere and floating object fountains*, see <http://www.kusser.com/>.

[3] See <http://midwarks.info/kenglobe/> for a highly readable report on the granite sphere fountain (also known as the "groovy ball project") in Kenilworth, UK.

[4] See the entry *Kugel ball* at <http://en.wikipedia.org/>, including the frequently-asked-questions section.

[5] Due to the extremely small thickness of the fluid layer, the water has hardly any freedom to explore the normal direction once it has left the nozzle region and is immediately forced into the parallel direction. As noted in Figs. 4 and 7, the size of the nozzle region covers only about 10% of the total range of θ. For the spherical fountain this constitutes an area of $\sim (0.1)^2 \sim 0.01$ of the total immersed area, making the contribution of the region that is not treated by our analysis of the order of 1%.

[6] G. G. Stokes, "On the effect of the internal friction of fluids on the motion of pendulums," Cambridge Philos. Trans. **9**, 8–106 (1851).

[7] G. K. Batchelor, *An Introduction to Fluid Dynamics* (Cambridge U.P., Cambridge UK, 1967). Flow fields in which inertia forces are negligible (including lubrication flows) are discussed in Sec. 4.8.

[8] F. M. White, *Viscous Fluid Flow*, 2nd ed. (McGraw-Hill, New York, 1991). Creeping flows (including lubrication flows) are discussed in Sec. 3-9.

[9] A. Cameron, *Basic Lubrication Theory*, Ellis Horwood Series in Engineering Science (Ellis Horwood, New York, 1976).

[10] O. Reynolds, "On the theory of lubrication and its application to Mr. Beauchamp Tower's experiments including an experimental determination of the viscosity of olive oil," Philos. Trans. Roy. Soc. London Ser. A **177**, 157–234 (1886).

[11] Y. A. Çengel and J. M. Cimbala, *Fluid Mechanics: Fundamentals and Applications* (McGraw-Hill, New York, 2006). The creeping flow approximation is treated in Sec. 10-3.

[12] L. G. Leal, *Advanced Transport Phenomena: Fluid Mechanics and Convective Transport Processes* (Cambridge U.P., Cambridge, 2007). The thin-gap approximation and lubrication problems are discussed in Chapter 5.

[13] J. Armengol, J. Calbó, T. Pujol, and P. Roura, "Bernoulli correction to viscous losses: Radial flow between two parallel discs," Am. J. Phys. **76**, 730–737 (2008).

[14] D. Quéré, "Leidenfrost Dynamics," Annu. Rev. Fluid Mech. **45**, 197–215 (2013).

[15] J. H. Snoeijer, P. Brunet, and J. Eggers, "Maximum size of drops levitated by an air cushion," Phys. Rev. E **79**, 036307 (2009).

[16] A photograph of the prizewinning airborne kugel can be found on the website of Brahma Granitech at <http://www.brahmagranitech.com/>.
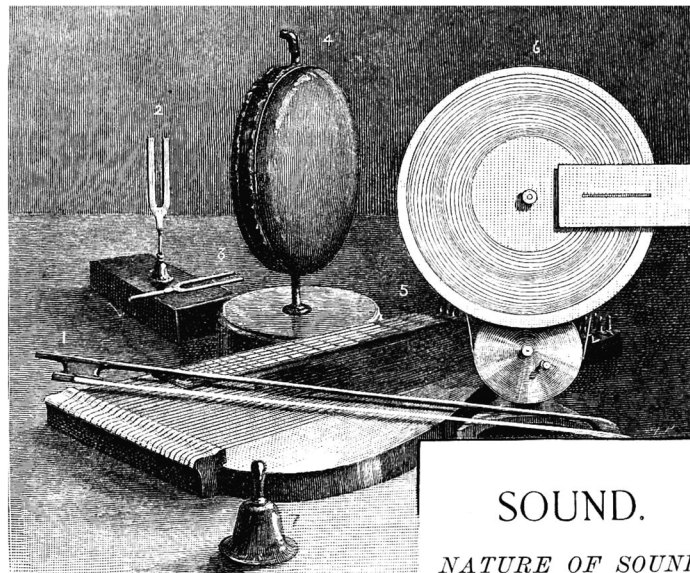
Acoustics Chapter Header

"Let the student provide himself with the articles [in the illustration]. No. 1 is a violin bow; 2, a tuning fork on a resonant box; 3, a C tuning fork; 4, a sound lens; 5, a zither; 6, a rotator; and 7, an ordinary bell." Mounted on the rotator is a Crova's disk; when viewed through the narrow slot in the card the student can see a simulation of a sound wave as it passes through an elastic medium. The quote is from John D. Quackenbos, Alfred M. Mayer, *et al*, Appleton's' *School Physics*, (American Book Company, New York, 1891), pg 370 (Notes by Thomas B. Greenslade, Jr., Kenyon College)